ISIJ International, Vol. 55 (2015), No. 10, pp. 2217–2224

Effect of Nb Microalloying on Reversion and Grain Growth in a High-Mn 204Cu Austenitic Stainless Steel

Anna KISKO,[1)]* Juho TALONEN,[2)] David Arthur PORTER[1)] and Leo Pentti KARJALAINEN[1)]

1) Centre for Advanced Steels Research, University of Oulu, P.O. Box 4200, Oulu, FI-90014 Finland.
2) Outokumpu Oyj, P.O. Box 140, Riihitontuntie 7B, Espoo, FI-02201 Finland.

(*Received on March 24, 2015; accepted on June 17, 2015*)

Highly refined grain size can be obtained in metastable austenitic stainless steels by martensitic reversion treatment, but the annealing must be controlled due to the high coarsening tendency of ultrafine grains. The effect of Nb microalloying on reversion and retardation of grain growth has been investigated in an austenitic 204Cu stainless steel containing Nb from 0 to 0.45 wt.%. Hot-rolled samples were cold rolled to a 60% reduction, leading to the formation of 47–60% strain-induced martensite, and subsequently annealed at various temperatures between 973 and 1 373 K up to 1 000 s. Grain size and precipitate structures were examined with optical, scanning and transmission electron microscopes. In the Nb-bearing steels, precipitate particles were found to retard the reversion. The reversion could be completed even at the low temperature of 973 K, but at 973–1 073 K the structure remained non-uniform consisting of fine reversed austenite grains and coarser grains with different degree of recrystallization. More uniform grain size in the range of 2–9 μm was obtained by reversion treatment at 1 173–1 373 K for 1 s, the grain size decreasing with increasing Nb content. Grain growth was effectively retarded by 0.28 wt.% Nb alloying even at 1 373 K and by 0.11 wt.% Nb at 1 273 K. The activation energy for grain growth increases with increasing Nb content from 363 to 458 kJ/mol. Zener's model and the flexible boundary model for the driving and pinning forces, respectively, can explain the observed retardation of grain growth.

KEY WORDS: austenitic stainless steel; niobium microalloying; precipitation; reversion treatment; recrystallization; grain growth; activation energy; pinning force; driving force.

1. Introduction

The steel industry is interested in developing high strength steels for lightweight applications. Typically, austenitic stainless steels have good ductility and formability but their yield strength is quite low.[1)] There are several methods to improve the strength, *e.g.*, solid solute strengthening, work hardening and grain size refinement.[2)] Many austenitic stainless steels are metastable at the room temperature so that during cold working some strain-induced martensite (SIM) forms, thereby increasing their strength[3)] but reducing ductility.[2)] Therefore, other strengthening methods such as grain size refinement are preferred.[4–8)]

An ultrafine grain size can be obtained by heavy cold deformation to create a high fraction of SIM that during subsequent proper annealing treatment reverts back to austenite. Martensitic reversion has already been investigated and reported during the 1970's, as referred by Tomimura *et al.*[4)] They also noted the formation of a fine austenite grain size obtained from reversed martensite in their experimental Cr–Ni steels. Since then, grain refinement by the martensitic reversion treatment in both Cr–Ni and Cr–Mn austenitic stainless steels has been considered in numerous papers, as witnessed by the 18 references given by Behjati *et al.*[9)] Tomimura *et al.*[5)] showed that the transformation can be either a diffusion or shear type, depending on the contents of Cr and Ni (the Ni/Cr ratio) in very low C and N bearing austenitic stainless steels. Later Somani *et al.*[7)] extended the compositional dependence of the reversion type adopting the Cr- and Ni-equivalents including the elements Mo and C, N, Mn, Si, respectively. The influence of the reversion type on the microstructural evolution has been demonstrated in Cr–Ni steels.[5,7,10–12)] However, the influence of microalloying has been investigated only by Sadeghpour *et al.*[13)] in a 201L-Ti steel and very recently by Shirdel *et al.*[14)] in 304L type steel microalloyed with Mo, Ti, V and Nb.

A precisely controlled reversion can provide an ultrafine grain size, but the duration of the annealing cycle is critical in the practical processing, for during annealing rapid grain growth tends to occur readily.[6,7,15)] Therefore, for a more robust annealing stage, the prevention or retardation of grain growth becomes important.

The driving force for grain growth is the energy stored in the material connected with grain boundaries. When the driving force exceeds the pinning force, the boundary will be mobile and grain growth can take place.[16)] A high pinning force is achieved by a large volume fraction of fine particles. Several authors have studied the effect of microalloying on grain size in carbon steels,[17–20)] but only few deal

* Corresponding author: E-mail: anna.kisko@oulu.fi
DOI: http://dx.doi.org/10.2355/isijinternational.ISIJINT-2015-156

with austenitic stainless steels,[21,22] especially in the instance of ultrafine grain size. Sawada *et al.*[23] studied the effect of V, Nb and Ti additions on the grain size refinement in type 301L 17Cr-7Ni austenitic stainless steel and demonstrated how microalloying can even lead to submicron grain sizes. They did not study grain growth, however. Only Sageghpour *et al.*[13] have investigated the influence of Ti alloying on the formation of nanocrystalline structure in type 201L 17Cr-7Mn-4Ni austenitic stainless steel and found that precipitation of nanosized TiC particles during the reversion annealing could retard the reversion process and suppress the subsequent grain growth. Hence, there is still a need for further investigations into the formation and stabilization of ultrafine grain structure in microalloyed austenitic stainless steels by the reversion and recrystallization processes. The aim of this work was to study the influence of Nb microalloying on the possibilities of obtaining uniform ultrafine grain size distributions after the reversion of SIM and recrystallization of cold-rolled retained austenite in type 204Cu (15Cr-9Mn-1Ni-2Cu) austenitic stainless steel.

2. Experimental

The material studied was in the form of sheets of an austenitic low-Ni Cr–Mn type 204Cu stainless steel without and with Nb microalloying delivered by Outokumpu Stainless Oy (Tornio, Finland). Their chemical compositions are listed in **Table 1**. The steel sheets (coded based on their Nb content) were cold rolled in a laboratory rolling mill to a 60% thickness reduction.

Pieces of the cold-rolled sheets were reversion annealed in a Gleeble 3800 thermo-mechanical simulator. The heating rate applied was 200 K/s, the annealing temperatures were 973, 1 073, 1 173, 1 273 and 1 373 K, and the holding times 1, 10, 100, 200 and 1 000 s. The cooling rate was 200 K/s down to 673 K followed by free cooling.

A Feritscope (Helmut Fisher FMP 30) instrument was employed to determine the SIM contents. The readings obtained were multiplied by a factor 1.7 for α'-martensite fractions as proposed in Ref. 24).

Grain sizes after annealing at various temperatures and times were examined using an optical microscope (OM), and the average grain size determined using the linear intercept method applied to the OM images. Further microstructural examinations were performed using a field emission scanning electron microscope (FE-SEM, Zeiss Ultra Plus) together with a Link Opal electron backscatter diffraction (EBSD) device (Oxford Instrument HKL, Channel5 software) and a transmission electron microscope (FETEM, LEO 912). For EBSD, the samples were polished using a diamond suspension down to 1 μm after which a chemical polishing was applied using a 0.05 μm colloidal silica suspension. For SEM, the samples were electrolytically etched with 6 V for 10 s using 10% oxalic acid. For SEM and EBSD, the accelerating voltages were 5 and 15 kV and the working distances 4.9–5 mm and 14.3–15.4 mm, respectively. The step size varied with the magnification, being 0.5 μm for 600X, 0.15 μm for 2000X, 0.05 μm for 5000X and 1000X. For the grain size analysis in EBSD, the threshold value of 0.3 μm as the minimum grain size accounted was used. The extraction replicas for examination of the precipitate particles in TEM were prepared by chemical etching of the specimens with 1% Nital for 5 s followed by the deposition of a vanadium film on the etched surface. The film was finally electrolytically removed with 10% nitric acid – ethanol solution.

Table 1. Chemical composition of the studied Nb microalloyed 204Cu steels [wt.%].

Steel	C	Si	Mn	Cr	Ni	Cu	N	Nb	Fe
0Nb	0.079	0.40	9.00	15.2	1.10	1.68	0.115	–	bal.
0.05Nb	0.070	0.30	9.13	15.2	1.10	1.70	0.165	0.05	bal.
0.11Nb	0.072	0.28	9.18	15.2	1.10	1.74	0.130	0.11	bal.
0.28Nb	0.083	0.28	9.19	15.1	1.10	1.74	0.160	0.28	bal.
0.45Nb	0.100	0.30	8.90	15.2	1.10	1.70	0.160	0.45	bal.

3. Results

According to ThermoCalc calculations for the 0.45Nb steels, **Fig. 1**, Nb(C,N) precipitates will be an equilibrium phase in the austenite at very high temperatures, right up to the liquidus temperature, and indeed they were observed by Pulkkinen *et al.*[25] in a 204Cu steel containing 0.45% Nb. **Figure 2** shows that coarse precipitates also exist in the present Nb microalloyed materials after cold rolling before the reversion treatment. Figure 1 suggests that below 1 373 K, also $M_{23}C_6$, Cr_2N, a Cu-rich phase and sigma phase are thermodynamically stable. However, the precipitation kinetics can be very slow.[26]

In the cold-rolling stage, SIM was formed so that after the 60% reduction, the sheets 0Nb, 0.05Nb, 0.11Nb, 0.28Nb and 0.45Nb contained 60, 53, 63, 47 and 49% of strain-induced α'-martensite, respectively. The fractions of

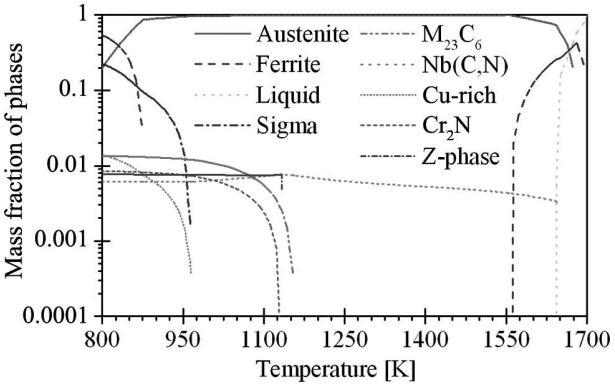

Fig. 1. Equilibrium mass fraction of various phases as a function of temperature for the 0.45Nb steel.

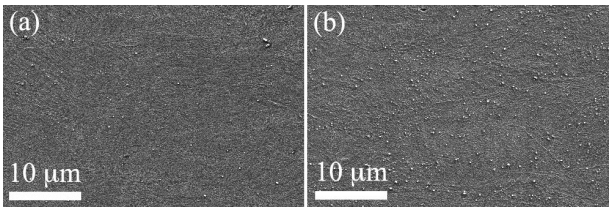

Fig. 2. SEM images of two steels after cold rolling revealing the presence of coarse precipitates, (a) 0.28Nb and (b) 0.45Nb.

SIM varied slightly. However, the influence of Nb on the stability of austenite is not clear. According to Lee *et al.*[27] Nb precipitates enhanced SIM formation in the beginning of tensile tests even though the total volume fraction of SIM after fracture was almost the same with or without Nb precipitates. Moreover, in the 0.28Nb and 0.45Nb steels, the carbon content is slightly higher than in the 0Nb and 0.11Nb steels. Carbon stabilizes the austenite phase,[28] so this might explain the lower martensite fractions obtained particularly in these two steels, but because the alloying with niobium leads to the formation of niobium carbides, which reduce the carbon content in solution, the austenite stability should be decreased. In the 0Nb steel all carbon and nitrogen are in solid solution, which should decrease the formation of SIM, but not observed. Hence, this calls for further studies.

Regarding the microstructure, it can be mentioned that according to the X-ray diffraction analysis (not shown here), the cold-rolled 0Nb steel contained also about 8% epsilon (hcp)-martensite. However, it is known that this martensite reverts to austenite at much lower temperatures as the SIM does,[29] so in practice during annealing we have two operative processes, the reversion of SIM and recrystallization of retained austenite, hence we neglected the presence of minor amount of epsilon-martensite.

Figure 3 presents the volume fraction of SIM content of the steels measured after the reversion treatment carried out at the lowest annealing temperature of 973 K. Reversion became complete (95% or more) during 1 000 s of soaking, in agreement with the previous study on the 0Nb steel.[30] However, a distinct retarding effect of Nb microalloying can be seen, most pronounced in the 0.11Nb steel and at the shortest holding times. A retardation of the reversion kinetics was observed by Sageghpour *et al.*[13] by Ti alloying in a 201L type steel. The slower reversion kinetics might be a result of fine precipitates which obstruct the nucleation of new austenite grains in martensite, even though the driving force for the reversion at 973 K is much higher than the pinning force of the precipitate particles. And why they are most effective in the 0.11Nb steel, calls for further study.

It is known from previous studies that in the 204Cu steel the martensite reversion becomes completed at 1 073 K within 1 s.[30] However, retained cold-deformed austenite grains are only recovered or partially recrystallized in that stage. Therefore, some grains still have their original larger diameter (recovered grains), while some are quite fine (recrystallized or reverted ones), *i.e.*, the grain size tends to become non-uniform during this reversion treatment, as exemplified for the 0Nb and 0.45Nb steels in **Figs. 4**(a), 4(c). Longer, 100 s soaking time at 1 073 K is needed to complete the recrystallization for the 0Nb steel, Fig. 4(b). After 10 s annealing, the average grain size was 1.44 μm and 1.07 μm for the 0Nb and 0.45Nb steels respectively, obtained from EBSD grain size distributions, but the structure contained large recovered grains, with the average grain size of 8.2 and 7.4 μm, and fine reverted grains, with the average grains size of 1.40 μm and 1.04 μm for the 0Nb and 0.45Nb steels, respectively. In the instance of the 0Nb steel, 1.6 μm grain size was detected after complete recrystallization, *i.e.*, after 100 s soaking. Niobium retards the recrystallization rate of retained austenite, for after 100 s soaking at 1 073 K there were still recovered grains in the 0.45Nb steel (Fig. 4(c)) whereas in the 0Nb steel the structure was already recrystallized (Fig. 4(b)). The grain size becomes uniform at 1 173 K annealing for 10 s, as exemplified for the 0Nb steel, Fig. 4(d). Hence, in order to obtain a more uniform grain size, soaking at higher temperatures than 1 073 K is preferred even though then some grain growth tends to take place.

In order to analyze the grain growth kinetics, grain sizes of the steels annealed at 1 173, 1 273 and 1 373 K were measured by the linear intercept method from OM images, and these results are plotted in **Fig. 5**. As seen, the grain sizes of 2–9 μm were obtained after annealing the 60% cold-rolled pieces for 1 s at 1 173 – 1 373 K. This grain size increased with increasing temperature and decreased with increasing Nb content of the steel. The grain size tends to grow with the continuing annealing, so that in the 0Nb steel, the initial grain size of 2 μm grew to 5 μm already within 100 s at 1 173 K. However, the growth remained much less in the Nb-bearing steels. From the data in Fig. 5, it can be concluded that the inhibition of grain growth by Nb microalloying becomes efficient with 0.11 wt.% Nb at temperatures

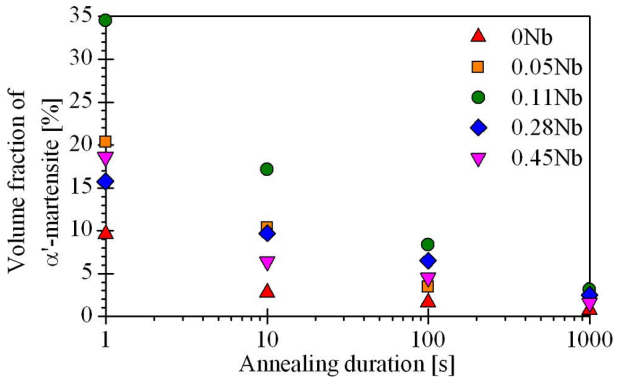

Fig. 3. The α'-martensite content of the 0–0.45Nb steels after annealing at 973 K for various durations. (Online version in color.)

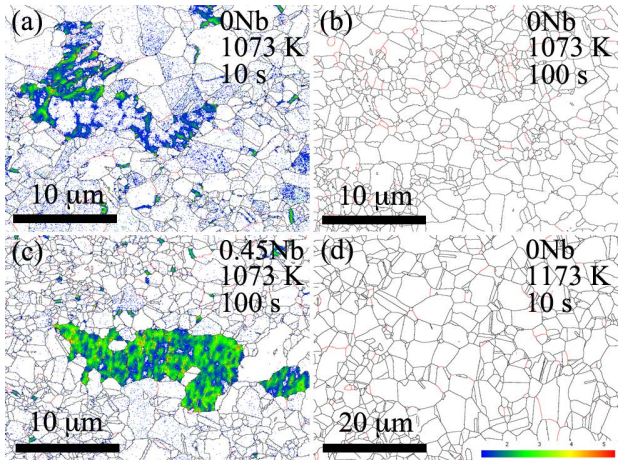

Fig. 4. EBSD grain boundary and kernel average misorientation (KAM) for the (a, b, d) 0Nb and (c) 0.45Nb steels after the cold rolling and annealing at (a–c) 1 073 K and (d) 1 173 K for (a, d) 10 s and (b, c) 100 s. The recovered areas are as colored, and black and red colored boundaries have misorientation higher than 15° and 3°, respectively. Note the different magnification in (a–c) from that in (d). (Online version in color.)

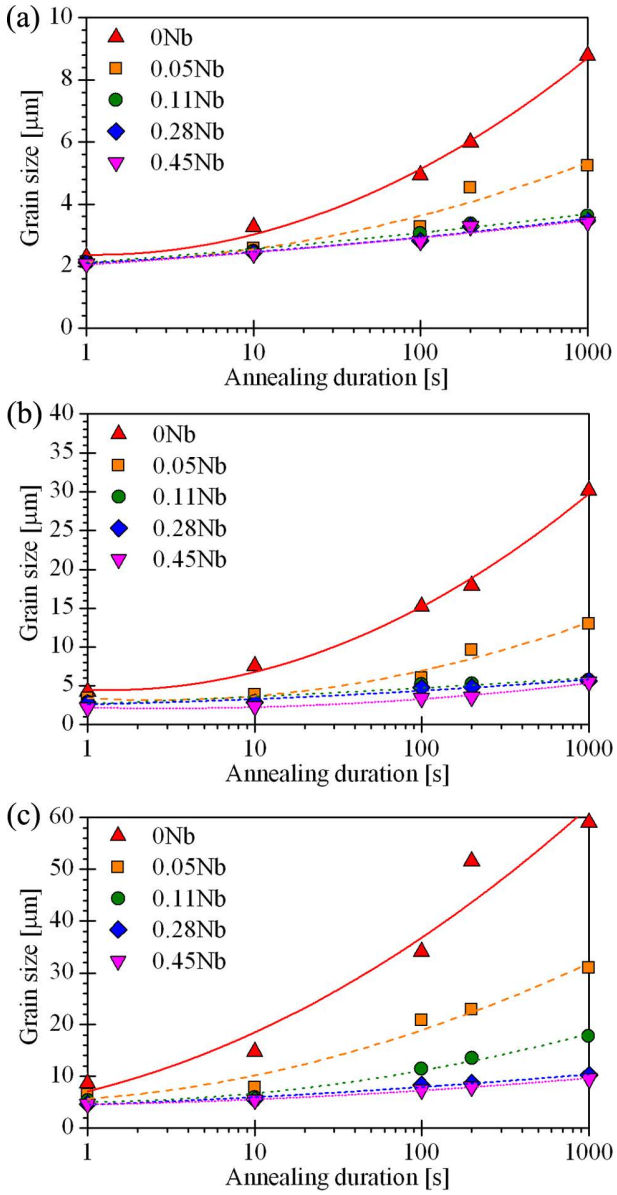

Fig. 5. Average grain size vs annealing duration of the samples annealed at (a) 1 173 K, (b) 1 273 K and (c) 1 373 K. (Online version in color.)

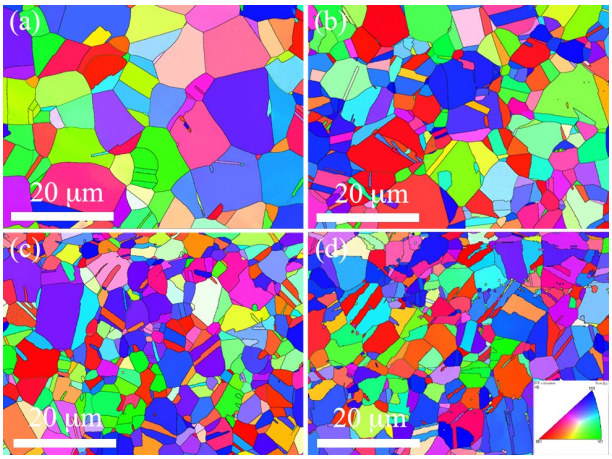

Fig. 6. EBSD IPF-X and grain boundary maps after the cold rolling and annealing at 1 373 K for 1 s. (a) 0Nb, (b) 0.11Nb, (c) 0.28Nb and (d) 0.45Nb. The black and green colored boundaries have misorientation higher than 15° and 3°, respectively. (Online version in color.)

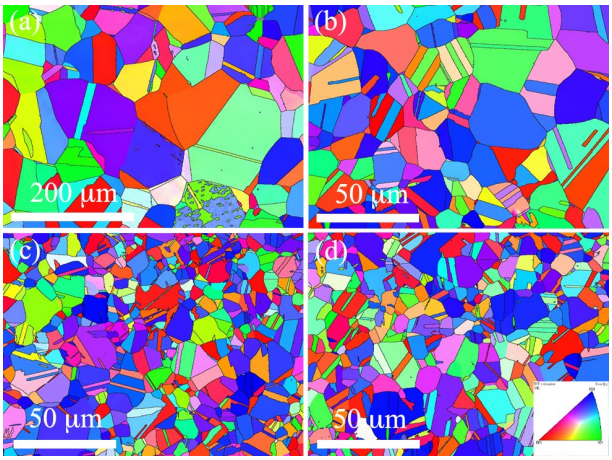

Fig. 7. EBSD IPF-X and grain boundary maps after the cold rolling and annealing at 1 373 K for 1 000 s. (a) 0Nb, (b) 0.11Nb, (c) 0.28Nb and (d) 0.45Nb. The black and green colored boundaries have misorientation higher than 15° and 3°, respectively. Note the different magnification in (a) from that in (b–d). (Online version in color.)

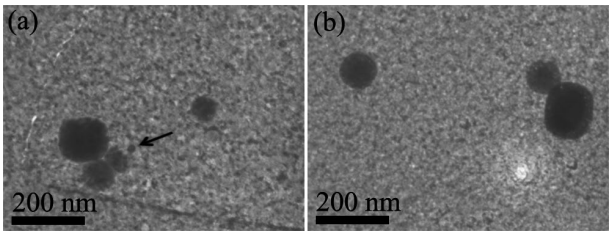

Fig. 8. TEM extraction replicas of the 0.45Nb steel after annealing at 1 373 K for (a) 1 s and (b) 1 000 s. In (a) a fine particle is pointed out with an arrow.

of 1 173–1 273 K and with 0.28 wt.% Nb at 1 373 K, and it remains such at the higher Nb contents.

Figures 6 and **7** illustrate the grain structures for the studied steels after annealing for 1 and 1 000 s, respectively, at 1 373 K, the highest temperature studied. After 1 s annealing, the grain size was less than 9 μm in all the steels but further refinement by increasing Nb microalloying can be seen. During 1 000 s, differences in the grain structures have appeared so that grain coarsening is obvious in some of the steels. The grain growth took place by normal grain growth, and abnormal grain growth was not observed at any annealing treatments.

From Figs. 1 and 2, it can be seen that the precipitation had already taken place in the course of hot rolling. Hence, these particles might tend to grow and possibly partly dissolve at high reversion annealing temperatures. Pulkkinen *et al.*[25] observed that the NbC and Nb(C,N) precipitation structure did not change in the 0.45Nb steel even during annealing up to 10 h at 1 173–1 273 K. Anyhow, the number and size of the particles at 1 373 K were examined here by extraction replicas in TEM. As an example, **Fig. 8** presents typical TEM images of the precipitation structure of the 0.45Nb steel after annealing at 1 373 K for 1 s (Fig. 8(a)) and 1 000 s (Fig. 8(b)). After the 1 s annealing particles with different sizes were seen; a fine particle pointed out with an arrow; but within the 1 000 s soaking the finest particles seemed to have disappeared.

Particle size analysis was performed using the images of TEM replicas by measuring manually the size of each particle. **Figure 9** shows particle radius distributions. The number of measured particles (N) is also given in the figure. It is seen that after 1 s soaking at 1 373 K, the number of fine particles (the radius less than 50 nm) was higher than after 1 000 s indicating particle coarsening. As the Nb content increases, the peak of the size distribution shifts slightly to larger particle sizes.

4. Discussion

As observed, ultrafine grain size (*i.e.*, a few micrometers in diameter) can be obtained in the studied 204Cu steels by 60% cold rolling and subsequent reversion annealing treatment. At 973 K the minimum grain size achieved is in the range of 0.5–1.5 μm. However, the grain structure is not uniform but consists of submicron-sized or micron-sized reverted grains and retained austenite grains, and also some α'-martensite. At 1 073 K, SIM has reversed back to austenite within 1 s, but after this short annealing the grain structure is inhomogeneous consisting of micron-sized reverted austenite grains and larger retained austenite grains (Fig. 4). Longer soakings can be utilized to recrystallize all austenite grains but the addition of Nb increases the time required for this, and the inhomogeneity in the structure seems to remain.

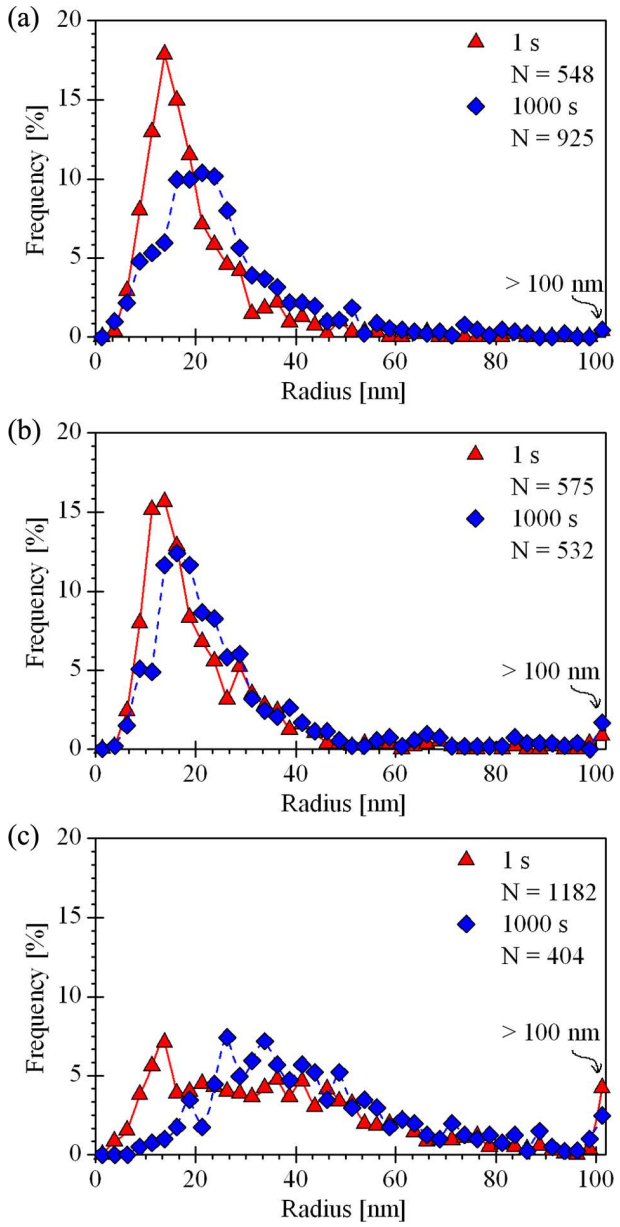

Fig. 9. Particle frequencies as a function of their radius for the (a) 0.11Nb, (b) 0.28Nb and (c) 0.45Nb steels annealed at 1 373 K. Number of measured particles (N) is given in the figures. (Online version in color.)

At temperatures of 1 173 K or higher, where reversion and also recrystallization are fast, the ultrafine and more uniform grain size can be obtained. Unfortunately then grain growth occurs, as ultrafine grains tend to coarsen with prolonged annealing, being 3 μm after 10 s at 1 173 K and 9 μm after 1 000 s in the 0Nb steel (Fig. 5). Rajasekhara *et al.*[6] reported the grain growth from 0.5 to 2.4 μm within holding from 1 to 10 s at 1 173 K in the 301LN Cr–Ni steel. Therefore, the prevention of grain coarsening or at least retarding it would be beneficial for practical processing. As shown by the data in Fig. 5, Nb microalloying seems to be an effective mean to obstruct grain growth. Also, it seems that 0.11 wt.% Nb is enough to retard the grain growth at 1 173–1 273 K, and 0.28 wt.% Nb even at 1 373 K. In addition, distinctly finer initial grain sizes are obtained in these Nb-bearing steels within short (1 s) annealing at 1 273–1 373 K than in the Nb-free 204Cu steel. Analyzing the grain growth data will bring about better understanding these observations, sections 4.1 and 4.2.

The steel 0Nb is alloyed with about 1.7 wt.% Cu, so that an issue is its possible segregation to grain boundaries and/or precipitation affecting the grain growth rate. It has been shown that the partitioning coefficient of Cu is close to 1, hence there is no special tendency of segregation in the solidification stage.[31] Jiao *et al.*[32] observed that Cu is even depleted at grain boundaries. Precipitation has been found to take place as intragranular nano-size metallic Cu particles.[33] However, the solubility of Cu in the austenite at 1 123 K is about 2.7 wt.%[32] and according to ThermoCalc calculations the solvus temperature of Cu in a 18Cr-9Ni-3Cu-Nb-N steel is 1 117 K.[34] According to Fig. 1, the solution temperature for the Cu-rich phase is 968 K in the 0.45Nb steel, so that no Cu precipitation is expected at annealing at temperatures of 973 K and above. Hence, we can conclude that Cu in the present steels is in the solid solution and does not cause differences in the grain growth kinetics between the steels.

4.1. Activation Energy for the Grain Growth

The kinetics of grain growth can be analyzed using the generalized grain growth law, Eq. (1):

$$(d - d_0)^n = kt \quad \text{..... (1)}$$

where d is the average grain size, d_0 the initial grain size (taken as 1 μm for all the steels), n the grain growth exponent, k the grain growth kinetic parameter and t the annealing time.[35] The grain growth exponent n and kinetic parameter k were estimated by linear regression analysis, **Fig. 10**.

As seen in Fig. 10(a), n values are in the range 3–8 increasing significantly with the Nb content and varying slightly with temperature being higher for lower annealing temperatures. A similar trend was observed by Rajasekhara and Ferreira.[36] Burke and Turnbull[37] have evaluated grain

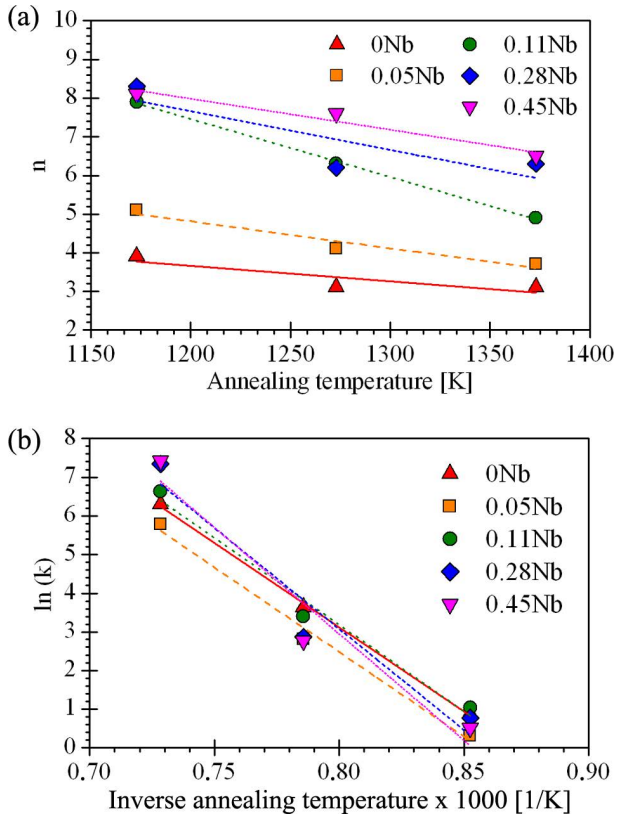

Fig. 10. Analysis of grain growth kinetics. (a) Grain growth exponent n and (b) kinetic parameter k vs. inverse annealing temperature. (Online version in color.)

growth in various metallic systems (microalloyed carbon steels, aluminum, brass) and also suggested that n increases with decreasing temperature. In theory, n is equal to 2 near the melting temperature for an ideal material with spherical grains without impurities.[16] For real materials, the grain growth exponent is typically greater than 2, because grains are not spherical and there are precipitates or chemical segregation at the grain boundaries that inhibit grain growth.[38] Rajasekhara and Ferreira[36] reported n values of 2.4–2.8 for 301LN stainless steel annealed at 1 073–1 273 K containing chromium nitride precipitates. These values are lower than the present ones for the 0Nb steel (n = 3.2−3.8). In the instance of the coupled grain growth and Ostwald ripening of second-phase particles in a binary system, the growth exponent should be equal to 3, independently of initial microstructures and the volume fraction of the second phase.[40] However, the present values of the higher Nb-bearing steels are much higher than 3. Higher exponents are found in the literature, for instance for an Fe-22Mn-0.6C steel, $n \approx 3.5$ has been reported.[39] Sabooni *et al.*[15] determined the grain growth exponent of 4.8 for reversion-treated ultrafine-grained 304L steel, decreasing with increasing annealing temperature. As discussed by them, nanocrystalline materials can show exponents up to 10.

The kinetic parameter k can be used to estimate the activation energy for the grain growth process, Eq. (2):

$$k = k_0 e^{\left(-\frac{\Delta G_{activation}}{RT}\right)} \quad \text{..... (2)}$$

where k_0 is a material constant, $\Delta G_{activation}$ the activation energy for grain growth, R the universal gas constant and T annealing temperature (in K).[35] The experimentally obtained values of k are plotted in Fig. 10(b). The value of ln(k) obtained for the 301LN stainless steel at 1 273 K was 3.6,[36] equal to the present value at 1 273 K for the 0Nb steel.

Table 2. Calculated activation energies [kJ/mol] of the steels.

Steel	0Nb	0.05Nb	0.11Nb	0.28Nb	0.45Nb
$\Delta G_{activation}$	363	364	373	435	458

Table 2 lists the calculated activation energies for the grain growth process. The 0Nb steel shows the lowest value of 363 kJ/mol. The activation energy for the grain growth seems to increase quite considerably with Nb microalloying, from 363 kJ/mol up to 458 kJ/mol. These higher values are comparable with the value of 435 kJ/mol reported for the austenite in a microalloyed Fe–C–Mn–Nb steel.[41] In fact, the reported experimental activation energies vary in a wide range 280–420 kJ/mol for type 321 and 347 austenitic stainless steels[21,42] and 455 kJ/mol for 304L.[15] Steels 321 and 347 contain stable TiC and NbC carbides, respectively, which create back-stress on grain boundaries hindering their motion, and they thereby increase the activation energy for grain growth.[38,43,44] This can be assumed to be the situation in the present steels, too.

4.2. Driving and Pinning Forces for Grain Growth

Grain size is controlled by the competition between the driving and pinning forces. The volume fraction of precipitates can be estimated either from replicas using the measured data for the mean particle size, the standard deviation of the size distribution and the precipitate number density[19] or calculated based on the chemical composition.[16] The values used to calculate the volume fraction of precipitates in this work are shown in **Table 3**. In this table, r is the mean radius of spherical particles smaller than 50 nm and s is the standard deviation of those particles. Mean particle sizes smaller than 50 nm are suggested to be effective for austenite grain boundary pinning[45] and therefore only these fine particles were used in the volume fraction and pinning force calculations.

The assumption for the theoretical calculations is that all Nb is bound in precipitates, either in NbC or NbN. **Table 4** compares the results of the experimental measurements and theoretical calculations.[16] As seen, the results are close to each other indicating that most of Nb added has precipitated as particles with a radius smaller than 50 nm in all the steels. The volume fractions estimated from the TEM replicas are used for the volume fractions in the calculations below.

Various models for the calculation of driving and pinning forces have been proposed in the literature. All of them are modifications of Zener's original expressions.[46] Here Eqs. (3)–(7) were used for the analyses, the expressions of Zener and Gladman (Eqs. (3) and (4), respectively) for calculating the driving forces and the Zener expressions (Eq. (5)), *i.e.* rigid boundary model (RBM) and flexible boundary model (FBM) (Eqs. (6)–(7), respectively) for the calculation of the pinning forces.[16,47]

$$F_d = \frac{2\gamma}{D} \quad \text{..... (3)}$$

Table 3. Data for the precipitates in the steels calculated from TEM data (r is the mean radius of particles smaller than 50 nm and s is the standard deviation).

Steel	Ann. time [s]	r [nm]	s [nm]
0.11Nb	1	18	16
	1 000	22	19
0.28Nb	1	19	18
	1 000	22	19
0.45Nb	1	29	31
	1 000	33	36

Table 4. Volume fraction of precipitates in the steels after annealing at 1 373 K for 1 or 1 000 s.

Steel	TEM study [%]		Theoretical calculation [%]
	1 s	1 000 s	
0.05Nb	0.05	0.02	0.055
0.11Nb	0.11	0.16	0.121
0.28Nb	0.29	0.26	0.308
0.45Nb	0.50	0.50	0.495

$$F_d = \left(\frac{3}{2} - \frac{2}{Z}\right)\left(\frac{\gamma}{D}\right) \quad \text{..... (4)}$$

$$F_p = \frac{3f\gamma}{2r} \quad \text{..... (5)}$$

$$F_p = \frac{6f\gamma}{\pi r} \quad \text{..... (6)}$$

$$F_p = \frac{3f^{2/3}\gamma}{\pi r} \quad \text{..... (7)}$$

In the Equations, γ is the grain boundary energy (taken as 0.8 J/m^2),[18] D the average radius of the grains, Z the size advantage, taken as 2, f the volume fraction of particles (taken from Table 4) and r the radius of the spherical particles. As seen from Fig. 8, Nb precipitates are approximately spherical so there is no need to convert their size to obtain the radius. The frequency data used in calculations are shown in Fig. 9.

The results of the calculations of both forces are shown in **Fig. 11**. The driving forces predicted by Gladman's expression are lower than those predicted by Zener's expression, because Gladman takes account for the size advantage of the growing grain in a matrix, whereas Zener presented the value of 2 in his equation.[16] The RBM for the pinning force assumes that the motion of a rigid boundary is capable of interacting only with those particles lying within ± r of the boundary plane (r is the radius of the particle). The FBM presumes that an infinitely flexible boundary can interact with every particle of radius r within a single plane of a three-dimensional array until fully pinned.[47] Therefore, the pinning forces predicted from the FBM are greater than those predicted from the RBM and Zener's expression, because a larger number of particles interact with the moving boundary in the FBM.[48]

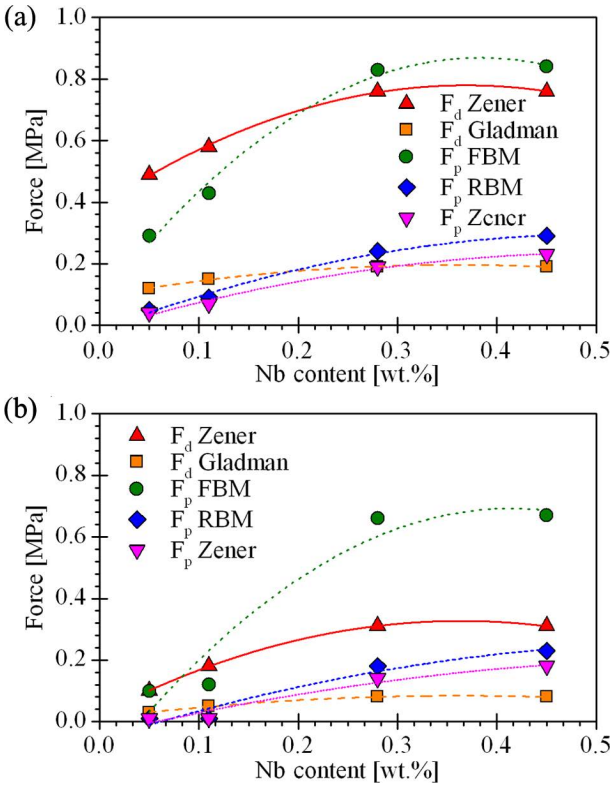

Fig. 11. Estimated driving (F_d) and pinning (F_p) forces for the steels after annealing at 1 373 K for (a) 1 s and (b) 1 000 s. (Online version in color.)

The comparison of pinning (F_p) and driving (F_d) forces, calculated from the above models, leads to different conclusions. For instance, F_p predicted by FBM is always higher than F_d predicted from Gladman, and therefore no grain growth should occur. However, if F_p is predicted from FBM and F_d predicted from Zener's equation, F_p is higher until the Nb content is at least 0.11 wt.%. The result is the same if F_p is predicted from Zener or RBM and F_d predicted from Gladman. Hence, these comparisons suggest that grain growth occurs in the 0Nb and 0.05Nb steels at 1 373 K. For the steels alloyed with 0.28 wt.% Nb or 0.45 wt.% Nb, pinning forces calculated by FBM are high, so that particles should prevent the grain coarsening. Hence, the Nb microalloying of 0.28 wt.% seems to be appropriate to achieve the maximum efficiency of the alloying. According to Fig. 11, the driving force in the 0.11Nb steel is slightly higher than the pinning force, and consistently we see from Fig. 5(c) that some grain coarsening takes place at 1 373 K, but hardly at lower temperatures. This result is also in agreement with the study by Sawada *et al.*[23] for an austenitic 301L stainless steel where they found that the Nb-addition of 0.1 wt.% is sufficient to prevent the grain coarsening of 2 μm grains during heat treatment at 1 123 K. When considering the evolution of the grain size with time, *e.g.* Fig. 5, some increase in grain size with increasing time is seen to be occurring up to the maximum studied 1 000 s. The reason for this is the fact that the pinning force is decreasing with time as the precipitate distribution coarsens.

5. Summary and Conclusions

Ultrafine austenite grain sizes were created by reversion annealing treatments of cold-rolled metastable Cr–Mn austenitic 204Cu stainless steel sheets containing 0–0.45 wt.% Nb. The kinetics of martensitic reversion and the stability of the grain size were followed after annealing at various temperatures. The following conclusions can be drawn from the work:

(1) Nb microalloying retards the start of martensite reversion at 973 K and the strongest influence is found with 0.11 wt.% Nb.

(2) At 1 073 K reversion is completed within 1 s, but then the grain structure consists of fine reversed and coarse retained austenite grains, some of which are recovered and some of which are partly recrystallized. Annealing for 100 s provides an average grain size smaller than 2 μm, but also coarser grains still exist as a result of recrystallization of the retained austenite grains.

(3) Highly refined grain sizes of 2–9 μm are obtained after annealing the 60% cold-rolled samples at 1 173–1 373 K for 1 s.

(4) Normal grain growth takes place during annealing at temperatures of 1 173 K and above, but microalloying with 0.11 wt.% Nb is sufficient to significantly retard the austenite grain coarsening up to 1 000 s at 1 273 K. To retard the grain coarsening up to 1 000 s at 1 373 K 0.28 wt.% Nb is required.

(5) The activation energy for the grain growth depends on the Nb content, increasing from 363 to 458 kJ/mol as the Nb content increases from 0 to 0.45 wt.%.

(6) Zener's model for the grain growth driving force and the flexible boundary model for the pinning force explain the observed grain coarsening behavior.

Acknowledgements

This work has been carried out within Finnish Metals and Engineering Competence Cluster (FIMECC Ltd) Breakthrough Steels and Applications (BSA) program and Light and Efficient Solutions program (FIMECC LIGHT, project 1) funded by the Finnish Funding Agency for Technology and Innovation (Tekes). The financial support from the Advanced Materials Doctoral Programme of the University of Oulu (ADMA-DP) is gratefully acknowledged. The authors would like to thank Outokumpu Stainless Oy for providing the experimental material. AK thanks Mr TunTun Nyo for his assistance in sample preparation.

REFERENCES

1) P. J. Cunat and T. Pauly: Proc. 4th European Stainless Steel Science and Market Cong., La Revue de Métallurgie, Paris, (2002), 10.
2) L. P. Karjalainen, T. Taulavuori, M. Sellman and A. Kyröläinen: *Steel Res. Int.*, **79** (2008), 404.
3) I. Tamura: *Met. Sci.*, **16** (1982), 245.
4) K. Tomimura, S. Takaki, S. Tanimoto and Y. Tokunaga: *ISIJ Int.*, **31** (1991), 721.
5) K. Tomimura, S. Takaki and Y. Tokunaga: *ISIJ Int.*, **31** (1991), 1431.
6) S. Rajasekhara, P. J. Ferreira, L. P. Karjalainen and A. Kyrolainen: *Metall. Mater. Trans. A*, **38A** (2007), 1202.
7) M. C. Somani, P. Juntunen, L. P. Karjalainen, R. D. K. Misra and A. Kyröläinen: *Metall. Mater. Trans. A*, **40A** (2009), 729.
8) A. Kisko, R. D. K. Misra, J. Talonen and L. P. Karjalainen: *Mater. Sci. Eng. A*, **578** (2013), 408.
9) P. Behjati, A. Kermanpur, A. Najafizadeh, H. Samaei Baghbadorani, L. P. Karjalainen, J.-G. Jung and Y.-K. Lee: *Metall. Mater. Trans. A*, **45A** (2014), 6317.
10) M. C. Somani, L. P. Karjalainen, A. Kyröläinen and T. Taulavuori: *Mater. Sci. Forum*, **539–543** (2007), 4875.
11) R. D. K. Misra, S. Nayak, P. K. C. Venkatasurya, V. Ramuni, M. C. Somani and L. P. Karjalainen: *Metall. Mater. Trans. A*, **41A** (2010), 2162.
12) R. D. K. Misra, Z. Zhang, P. K. C. Venkatasurya, M. C. Somani and L. P. Karjalainen: *Mater. Sci. Eng. A*, **528** (2011), 1889.
13) S. Sadeghpour, A. Kermanpur and A. Najafizadeh: *Mater. Sci. Eng. A*, **584** (2013), 177.
14) M. Shirdel, H. Mirzadeh and M. Habibi Parsa: *Metall. Mater. Trans. A*, **A45** (2014), 5185.
15) S. Sabooni, F. Karimzadeh and M. H. Enayati: *J. Mater. Eng. Perform.*, **23** (2014), 1665.
16) T. Gladman: Grain Size Control, Maney, London, (2004), 183.
17) I. Tamura, H. Sekine, T. Tanaka and C. Ouchi: Thermomechanical Processing of High Strength Low Alloy Steels, Butterworth and Company, London, (1988), 1.
18) M. Chapa, S. F. Medina, V. López and B. Fernández: *ISIJ Int.*, **42** (2002), 1288.
19) M. Gòmez, S. F. Medina and P. Valles: *ISIJ Int.*, **45** (2005), 1711.
20) Q. Sha and Z. Sun: *Mater. Sci. Eng. A*, **523** (2009), 77.
21) J. K. Stanley and A. J. Perotta: *Metallography*, **2** (1969), 349.
22) A. F. Padilha, J. C. Dutra and V. Randle: *Mater. Sci. Technol.*, **15** (1999), 1009.
23) M. Sawada, K. Adachi and T. Maeda: *ISIJ Int.*, **51** (2011), 991.
24) J. Talonen, P. Aspegren and H. Hanninen: *Mater. Sci. Technol.*, **20** (2004), 1506.
25) H. Pulkkinen, S. Papula, O. Todoshchenko, J. Talonen and H. Hänninen: *Steel Res. Int.*, **84** (2013), 1.
26) T. Sourmail: *Mater. Sci. Technol.*, **17** (2001), 1.
27) Y. K. Lee, J. E. Jin and Y. Q: Ma: *Scr. Mater.*, **57** (2007), 707.
28) U. Krupp, C. West and H. J. Christ: *Mater. Sci. Eng. A*, **481–482** (2008), 713.
29) D. P. Escobar, S. S. Ferreira de Dafé and D. B. Santos: *J. Mater. Res. Technol.*, **4** (2015), 162.
30) A. Kisko, A. Hamada, L. P. Karjalainen and J. Talonen: 1st Int. Conf. on High Manganese Steel, Research Institute of Iron and Steel Technology, Yonsei University, Seoul, (2011), B-19.
31) P. L. Ferrandini, C. T. Rios, A. T. Dutra, M. A. Jaime, P. R. Mei and R. Caram: *Mater. Sci. Eng. A*, **435–436** (2006), 139.
32) Z. Jiao and G. S. Was: *Acta Mater.*, **59** (2011), 1220.
33) K. Laha, J. Kyono and N. Shinya: *Scr. Mater.*, **56** (2007), 915.
34) C.-Y. Chi, H.-Y. Yu, J.-X. Dong, W.-Q. Liu, S.-C. Cheng, Z.-D. Liu and X.-S. Xie: *Prog. Nat. Sci.: Mater. Int.*, **22** (2012), 175.
35) D. A. Porter and K. E. Easterling: Phase Transformation in Metals and Alloys, 3rd ed., Chapman & Hall, London, (1990), 520.
36) S. Rajasekhara and P. J. Ferreira: *Acta Mater.*, **59** (2011), 738.
37) J. E. Burke and D. Turnbull: *Prog. Met. Phys.*, **3** (1952), 220.
38) M. Hillert: *Acta Metall.*, **13** (1965), 227.
39) A. Ferraiuolo, A. Smith, J. G. Sevillano, F. de las Cuevas, P. Karjalainen, G. Pratolongo, H. Gouveia and M. Mendes Rodrigues: Metallurgical Design of High-Strength Austenitic Fe-C-Mn Steels with Excellent Formability (METALDESIGN), EUR 25063 EN, European Union, Luxembourg, (2012), 46.
40) D. Fan and L. Chen: *J. Am. Ceram. Soc.*, **80** (1997), 1773.
41) P. D. Hodgson and R. K. Gibbs: *ISIJ Int.*, **32** (1992), 1329.
42) R. M. German: *Metallography*, **11** (1978), 235.
43) J. E. Spruiell, J. A. Scott, C. S. Ary and R. L. Hardin: *Metall. Trans. A*, **4** (1973), 1533.
44) M. F. Ashby and R. Ebeling: *Trans. Met. Soc. AIME*, **236** (1966), 1396.
45) R. L. Bodnar: *Iron Steelmaker*, **21** (1994), 19.
46) C. S. Smith: *Trans. Met. Soc. AIME*, **175** (1948), 15.
47) L. J. Cuddy: Proc. Int. Conf. on the Thermomechanical Processing of Microalloyed Austenite, The Metallurgical Society of AIME, Pittsburgh, (1982), 129.
48) O. Kwon and A. J. DeArdo: *Acta Metall. Mater.*, **39** (1991), 529.